THE JOURNAL OF PHYSICAL CHEMISTRY Letters

Letter

Cite This: J. Phys. Chem. Lett. 2020, 11, 88−92

pubs.acs.org/JPCL

Characterization of the Ground States of BeC_2 and BeC_2^- via Photoelectron Velocity Map Imaging Spectroscopy

Mallory L. Green, Noah B. Jaffe, and Michael C. Heaven*

Department of Chemistry, Emory University, Atlanta, Georgia 30322, United States

ABSTRACT: Due to their potentially unique properties, beryllium carbide materials have been the subject of many theoretical studies. However, experimental validation has been lacking due to the difficulties of working with Be. Neutral beryllium dicarbide has been predicted to have a T-shaped equilibrium structure (C_{2v}), while previous quantum chemistry calculations for the structure of the anion had not yielded consistent results. In this study, we report photoelectron velocity map imaging spectra for the BeC_2^- X $^2A_1 \rightarrow$ BeC_2 X $^1A_1$ transition. These data provide vibrational frequencies and the electron affinity of BeC_2. *Ab initio* electronic structure calculations, validated against the experimental data, show that both the anion and the neutral form have C_{2v} equilibrium geometries with polar covalent bonding between Be and the C_2 subunit. Computed vibrational frequencies and the electron affinity, obtained at the CCSD(T) level of theory, were found to be in good agreement with the measurements.

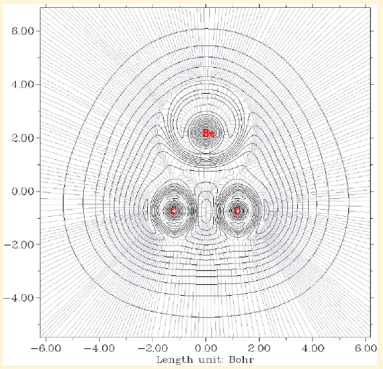

Metallized carbides exhibit a range of useful properties, not manifested by pure carbon materials, due to the unique characteristics of the doped metals. Beryllium is a very distinctive element known to exhibit more covalent bonding, as compared to other group IIa metals.[1−7] Beryllium carbides are of interest as graphene alternatives[8] and metallo-carbohydrenes.[9] Beryllium carbide clusters have been identified as promising materials for hydrogen storage in nanomaterials.[9] Also, there is interest in beryllium-doped carbon clusters as they have been found to be beneficial for the creation of thin films for use in nuclear and plasma sciences.[10] Under high pressures, BeC_2 has been shown to behave more as an insulator than an electrical conductor, counter to the behavior of the other alkaline earth metal dicarbides.[11] Given this background, investigation of the smallest beryllium carbide clusters is of interest as this can lead to a better understanding of bonding within the larger class of clusters and bulk materials.

Many dicarbide species have been investigated to explore the factors influencing bonding and equilibrium geometries. SiC_2[12] and GeC_2[13,14] have been found to exhibit bent (T-shaped) structures with predominantly $M^+-(C_2^-)$ ionic bonding (where Si and Ge are considered to be metalloids). This is a marked difference from the geometry of the non-metal−non-metal bonding of C_2P and C_2As, where the heteroatom bonds to the C_2 moiety in an end-on scheme, producing a covalent linear $C_{\infty v}$ molecule.[15] Many metallic dicarbides have been predicted to exhibit T-shaped structures with ionic character, including the heavier alkaline earth metals.[16,17] However, due to beryllium's tendency toward covalent bonding, there is the possibility that BeC_2 might not show the same degree of metallic bonding character as the other Group IIa metals.

Motivated by the quest to find the smallest cyclic molecule that could stabilize a C≡C bond, Frenking[6] carried out a careful theoretical analysis of the bonding in BeC_2. He found that the singlet T-shaped geometry was the minimum-energy configuration, with a C−C bond order close to 3. However, BeC_2 was not the example of a cyclic π-bonded system for which they had hoped. Instead, Frenking[6] concluded that the Be−C_2 bond was markedly ionic. He also noted that T-shaped BeC_2 would be stable in the gas phase. Subsequent theoretical studies have been consistent with these conclusions.[18−23] By contrast, there is very little information concerning the structure of the anion. Chen et al.[20] used hybrid B3LYP density functional theory to examine beryllium-doped linear carbon chains. Geometry optimizations were carried out using the Pople 6-31G* basis sets. They reported the ground state of BeC_2^- to be a linear structure, similar to that of the nonmetallic C_2P and C_2As.[15] Ghouri et al.[19] used the B3PW91 method with 6-31G* basis functions to investigate neutral Be_nC_m clusters, and they also reported vertical electron affinities (EAs) for the equilibrium geometries. For T-shaped BeC_2, they obtained a value near 2 eV, but they did not explore the minimum-energy structure for the anion. The density functional theory (DFT) calculations of Patrick et al.[22] (B3PW91 with large Pople-style basis sets of triple-ζ quality) predicted that linear geometry for the anion was not stable, and they obtained an adiabatic EA of 1.99 eV for T-shaped BeC_2.

In this study, we have used anion photodetachment spectroscopy and *ab initio* electronic structure calculations to examine the bonding and equilibrium geometries of both the neutral form and the anion. High-level electronic structure calculations were carried out to facilitate interpretation of the spectroscopic data and further analyses of the bonding.

Received: November 7, 2019
Accepted: December 10, 2019
Published: December 10, 2019

DOI: 10.1021/acs.jpclett.9b03297
J. Phys. Chem. Lett. 2020, 11, 88−92

Photoelectron spectra of the BeC_2^- $X\ ^2A_1 \rightarrow BeC_2$ $X\ ^1A_1$ transition were obtained using a velocity map imaging spectrometer, described previously.[24−27] Anions were generated through pulsed laser ablation of a beryllium rod into a flow of helium buffer gas, using the fundamental output of a Nd/YAG Minilite laser (1064 nm). The buffer gas was seeded with 1% acetylene to provide a source of carbon. Anions from the ablation plume were mass selected and subjected to photodetachment by a frequency-doubled Nd/YAG laser (532 nm) or an excimer-pumped tunable dye laser operating in the wavelength range of 532−643 nm. For all measurements, the lasers were vertically polarized.

Accumulated photoelectron images were processed using MEVELER.[28] Energy calibrations were conducted using the known electron detachment transitions of S^-, for photodetachment wavelengths ranging from 532 to 580 nm.

Figure 1 shows a processed velocity map image (inset) and the photoelectron spectrum recorded using 544.56 nm (18363 cm^{-1}) detachment photons. Assignment of this spectrum was guided by the results from electronic structure calculations that are described below. The numbering of the vibrational modes corresponds to the CC stretch (ν_1), the Be−C_2 stretch (ν_2), and the bending mode (ν_3).

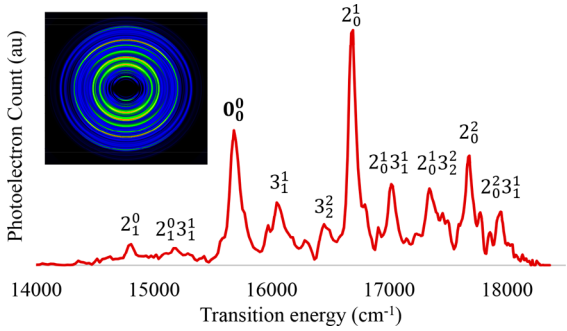

Figure 1. Photoelectron spectrum, and corresponding velocity map image, for the $BeC_2^- \rightarrow BeC_2$ transition, taken at a photodetachment energy of 18363 cm^{-1}. The transition energy is the photodetachment energy minus the electron kinetic energy.

Table 1 lists the assigned vibronic transitions. The energy for each assigned transition was obtained from an image recorded with the detachment photon energy set just above the specific appearance threshold to achieve the best resolution. The peak located at 15649 cm^{-1} was identified as the origin band, given its intensity and proximity to the predicted value of the electron affinity for T-shaped neutral BeC_2 (see Table 2). The other strong bands, located at relative energies of 991 and 2004 cm^{-1} from the origin, are assigned to the Be−C_2 stretch fundamental (ν_2) and first overtone ($2\nu_2$) of the neutral. The two peaks directly above the origin are the first and second $\Delta\nu_3 = 0$ bending sequence bands. Note that the ν_3 vibrational mode transforms as the B_2 irreducible representation in C_{2v} symmetry, so detachment events that involve odd changes in the ν_3 quantum number are symmetry forbidden.

Table 1. Peak Positions, Offsets from the Origin, and Vibronic Assignments for the $BeC_2^- \rightarrow BeC_2$ Spectra

energy (cm^{-1})	offset (cm^{-1})	assignment
14788	−861	2_1^0
15099	−550	$2_1^0 3_1^1$
15649	0	0_0^0
16031	382	3_1^1
16416	767	3_2^2
16640	991	2_0^1
16975	1326	$2_0^1 3_1^1$
17357	1708	$2_0^1 3_2^2$
17653	2004	2_0^2
17942	2293	$2_0^2 3_1^1$

Table 2. Comparison of the Experimentally Determined and Calculated Vibrational Constants for BeC_2

	observed (cm^{-1})	CCSD(T)
EA	15649 ± 39	15618[a]
ν_1	not active	1739
ν_2	998 ± 3	1054.1
$\nu_3 - \nu_3^-$	387 ± 7	398

[a]Includes zero-point energy correction.

The peaks located at 16975, 17357, and 17942 cm^{-1} are assigned to bend−stretch combination modes. The transitions at energies below the origin are the stretch hot band $\nu_2^- = 1$ and the bend−stretch combination hot band, respectively. The C−C stretch was not active in this spectrum, indicative of a very small difference in the C−C bond length between the neutral form and the anion. The experimentally and computationally determined electron affinities and vibrational constants are listed in Table 2.

Electronic structure calculations were carried out for the linear and bent geometries of the doublet states of the BeC_2^- anion and the singlet states of the BeC_2 neutral form, using RCCSD(T)/ CCSD(T) methods with aug-cc-pVQZ basis sets.[29] The Molpro 2010.1 computational package[30] was used for these predictions. Optimized geometries and vibrational frequencies of the anion and neutral species are listed in Table 3. This table also includes the electron affinity for the T-shaped and linear geometries of the neutral molecule, with zero-point energies taken into account. The C_{2v} structure was found to be the most stable isomer of the neutral form, by approximately 10000 cm^{-1}. This calculation was in good agreement with previous work.[6,16,18,19,21−23] The C_{2v} structure was found to be the most stable isomer for anion, which contradicts the findings of Chen et al.[20] The linear structure of the anion was predicted to exist only 1200 cm^{-1} above the bent geometry, for the anion.

To determine the barrier for conversion from the linear to the bent geometry, angular cuts through the potential energy hypersurface were constructed. Point-wise energies were calculated for variation of the ∠BeCC angle from 180° to 90° (linear to L-shaped, respectively). These curves are shown in Figure 2. For the anion, there is a barrier of approximately 640 cm^{-1}, indicating that the linear geometry could be stable at low temperatures. However, the neutral BeC_2 curve reveals a much smaller barrier supporting the linear geometry, suggesting that the linear neutral molecule is not stable. The work of Patrick et al.[22] gave similar relative energies for the neutral form but indicated that the linear state was slightly lower in energy, relative to the T-shaped minimum.[22] Dissociation energies for the $BeC_2 \rightarrow Be + C_2$ and $BeC_2^- \rightarrow Be + C_2^-$ processes (under C_{2v} symmetry) were predicted by the present coupled cluster calculations to be 40920 and 29890 cm^{-1}, respectively.

To examine the bonding characteristics of the anion and neutral form, natural bond orbital (NBO)[31] analyses were

DOI: 10.1021/acs.jpclett.9b03297
J. Phys. Chem. Lett. 2020, 11, 88−92

Table 3. Calculated Relative Energies, Optimized Geometries, and Vibrational Frequencies of the Linear and Bent Conformations of BeC_2 and BeC_2^-

	symmetry	state	EA (cm^{-1})	E_{rel} (cm^{-1})	r_{BeC} (Å)	r_{CC} (Å)	bond angle[a] (deg)	ν_1 (cm^{-1})	ν_2 (cm^{-1})	ν_3 (cm^{-1})
BeC_2	$C_{\infty v}$	$^1\Sigma^+$	24223	10062	1.562	1.267	180	1714.7	823.6	102.9
	C_{2v}	$^1A_1$	15361	0	1.616	1.275	46.4	1739.4	1054.1	674.1
BeC_2^-	$C_{\infty v}$	$^2\Sigma^+$	–	1200	1.591	1.269	180	1910.6	931.5	151.2
	C_{2v}	$^2A_1$	–	0	1.724	1.272	43.3	1784.0	893.7	275.7

[a]The bond angle for linear $C_{\infty v}$ structures is defined as ∠BeCC, and the bond angle for the bent C_{2v} structures is defined as ∠CBeC.

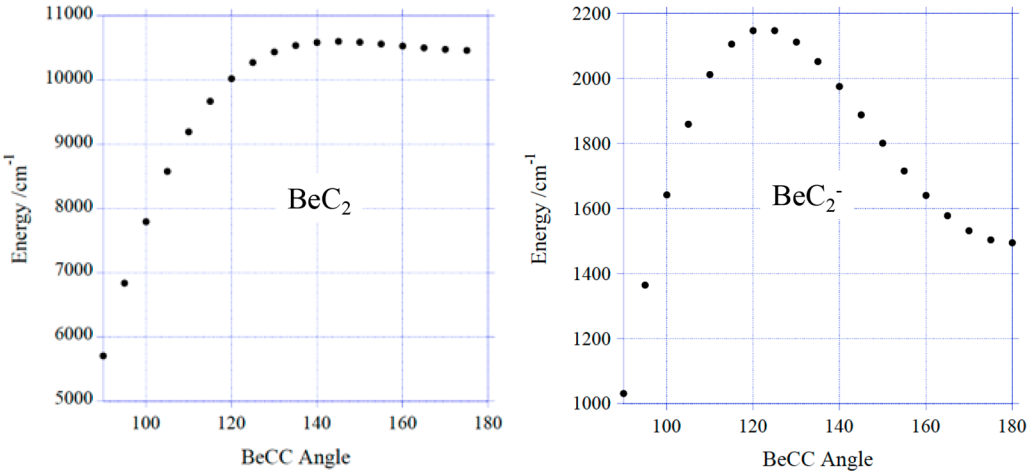

Figure 2. Angular cuts of the potential energy surfaces of BeC_2 and BeC_2^-. Energies are relative to the global minimum for each potential energy surface. The bond lengths were fixed at r_{CC} = 1.27 Å and r_{BeC} = 1.60 Å.

performed and localized orbital locator function (LOL)[32,33] surfaces were constructed. NBO analyses of the anion and neutral ground states were implemented using the Gaussian 09 program, using DFT with the B3LYP functional and 6-311++G Pople basis sets.[34] NBO results for the neutral molecule indicated a triple bond between the two carbon atoms and a single bond from each carbon to the beryllium atom. The Be−C bonds were primarily comprised of carbon hybrid orbitals, as the bonds were >80% C 2s/2p and <20% Be 2s/2p character. The NBO analysis of the anion also indicated a C≡C bond, but the level of bonding to the Be atom was decreased to the point where the effective Be−C bond order was 0.75.

A more nuanced picture of the bonding was obtained by using the Multiwfn software package[33] to analyze the wave functions. Panels a and b of Figure 3 show plots of the localized orbital locator function for the neutral form and the anion, respectively. The bond critical points are also shown as dots that are located on the C_2 rotation axis. For both the neutral molecule and the anion, there is an obvious build-up of electron density between the carbon atoms with the expected bond critical point between them. For the neutral molecule, the C−C bond orders obtained from the Mayer and Fuzzy Bond Order (FBO)[33,35] indices were 1.6 and 2.3, respectively. Note that the calculated vibrational frequency was consistent with a double bond. The frequency was lower than that of diatomic C_2 (ω_e = 1845.71 cm^{-1}) by just 106 cm^{-1}. The Mulliken and Hirshfeld atomic charges were −0.24 and −0.23 for C and 0.48 and 0.46 for Be, respectively (the electron-depleted region around Be is evident in Figure 3a). This charge distribution and the position of the second bond critical point indicate that the bonding between Be and the C_2 moiety is of a polar covalent type, with a large contribution from the electrostatic interactions. These conclusions are in agreement with the analysis given by Frenking[6] and differ only in the rather model-dependent matter of the C−C bond order. Animation of the vibrational modes further supports the model of polar covalent bonding for the Be atom. The bending vibration involves a minimal change in the C−C bond length and is best described as a libration of the C_2 subunit, such that Jacobi coordinates are the appropriate choice for discussion of the vibrational motions.

In our previous studies of the BeO^- and BeS^- anions, we found that the additional electron of the anion was accommodated by Be 2s/2p hybrid orbitals that were polarized away from the negatively charged O or S atom.[24,25] BeC_2 is similar to BeO/BeS in that the ionic bonding can be formally represented as $Be^{2+}X^{2-}$. In keeping with this view, we found that the additional electron of BeC_2^- resides in a back-polarized, Be-centered, in-plane 2s/2p hybrid orbital. This can be seen in Figure 3b, where there is increased electron density localized above the Be atom, with some additional negative charge that has been pushed onto C_2. The charge distribution has become (Mulliken and Hirshfeld) −0.12 and −0.18 on Be and −0.44 and −0.41 on each C, respectively. The partial negative charge on Be diminishes the attraction to C_2, resulting in a lengthening of the Be−C_2 Jacobi distance from 1.49 to 1.60 Å. This change is accompanied by significant decreases in the Be−C_2 stretch and bend frequencies. The transfer of charge into the LUMO of C_2 results in a slightly higher C−C stretch frequency but almost no change in the C−C bond length (cf. Table 3). Overall, these changes in geometry explain why the Be−C_2 stretch was active in the photodetachment spectrum while the C−C stretch was not. Note that the bond critical points are in similar positions for both BeC_2 and BeC_2^-, indicating that the Be−C_2^- bond is still polar covalent with strong electrostatic contributions. The bond orders for the

DOI: 10.1021/acs.jpclett.9b03297
J. Phys. Chem. Lett. 2020, 11, 88−92

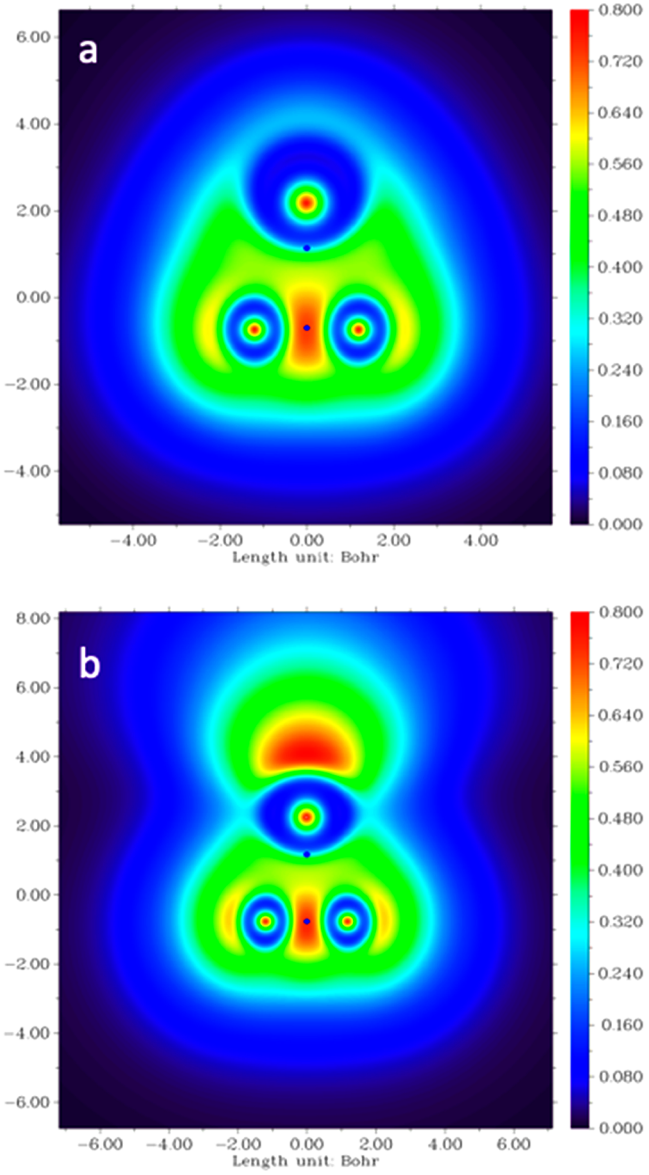

Figure 3. Cross section of the LOL surfaces for (a) BeC_2 and (b) BeC_2^-. The two bond critical points on the C_{2v} rotation axis are indicated.

anion were 1.6 (C−C) and 0.75 (Be−C) for the Mayer model and 1.2 (C−C) and 0.48 (Be−C) for the FBO model. The decrease in the C−C bond order (as compared to that of the neutral form) for the FBO was unexpected and may be an artifact of the application of this approximation to an open-shell system.

In conclusion, anion photodetachment measurements have provided the first experimental data for BeC_2 and the BeC_2^- anion. In accord with previous theoretical studies, the structure of BeC_2 is found to be T-shaped, with a polar covalent bond between Be and C_2. The structure of the anion was also found to be T-shaped, resolving a previous disagreement between predictions. *Ab initio* coupled calculations, validated against the experimental data, indicted a double bond for the C_2 subunit for both the neutral molecule and the anion. The Be−C_2^- bond of the anion was also found to be polar covalent but weakened (relative to that of the neutral form) by the additional neagative charge. The calculated EA was found to be in excellent agreement with the measured value of 1.905 eV.

AUTHOR INFORMATION

Corresponding Author

*E-mail: mheaven@emory.edu. Phone: (404) 727-6617.

ORCID

Michael C. Heaven: 0000-0003-4738-2408

Notes

The authors declare no competing financial interest.

ACKNOWLEDGMENTS

This material is based upon work supported by National Science Foundation Grant CHE-1565912. The authors also extend a special thanks to Mr. Sean Bresler for his assistance in troubleshooting the instrumentation.

REFERENCES

(1) Green, M. L.; Jean, P.; Heaven, M. C. Dative Bonding Between Closed-Shell Atoms: The BeF^- Anion. *J. Phys. Chem. Lett.* **2018**, *9*, 1999−2002.

(2) Heaven, M. C.; Merritt, J. M.; Bondybey, V. E. Bonding in Beryllium Clusters. *Annu. Rev. Phys. Chem.* **2011**, *62*, 375−93.

(3) Heaven, M. C.; Bondybey, V. E.; Merritt, J. M.; Kaledin, A. L. The Unique Bonding Characteristics of Beryllium and the Group IIA Metals. *Chem. Phys. Lett.* **2011**, *506*, 1−14.

(4) Merritt, J. M.; Bondybey, V. E.; Heaven, M. C. Spectroscopy, Structure, and Ionization Energy of BeOBe. *J. Phys. Chem. A* **2009**, *113*, 13300−13309.

(5) Merritt, J. M.; Bondybey, V. E.; Heaven, M. C. Beryllium Dimer-Caught in the Act of Bonding. *Science* **2009**, *324*, 1548−1551.

(6) Frenking, G. Carbon-Carbon Triple-Bond Stabilization in Three-Membered Ring Compounds: Boriryne, Dilithiumcyclopropyne and Berylliryne. *Chem. Phys. Lett.* **1984**, *111*, 529−32.

(7) Frenking, G.; Koch, W.; Gauss, J.; Cremer, D. Stabilities and Nature of the Attractive Interactions in HeBeO, NeBeO, and ArBeO and a Comparison with Analogs NGLiF, NGBN, and NGLiH (NG = He, Ar). A Theoretical Investigation. *J. Am. Chem. Soc.* **1988**, *110*, 8007−16.

(8) Zaleski-Ejgierd, P.; Hakala, M.; Pyykko, P. Comparison of Chain Versus Sheet Crystal Structures for Cyanides MCN (M = Cu-Au) and Dicarbides MC_2 (M = Be-Ba; Zn-Hg). Alternatives to Graphene? *Phys. Rev. B: Condens. Matter Mater. Phys.* **2007**, *76*, 094104.

(9) Tuerker, L. Hydrogen Storage Capacity of Be@C115 System. *J. Mol. Struct.: THEOCHEM* **2005**, *723*, 105−110.

(10) Xie, Y.; Morosoff, N. C.; James, W. J. XPS Characterization of Beryllium Carbide Thin Films Formed via Plasma Deposition. *J. Nucl. Mater.* **2001**, *289*, 48−51.

(11) Du, H.; Feng, W.; Li, F.; Wang, D.; Zhou, D.; Liu, Y. Nonmetallization and Band Inversion in Beryllium Dicarbide at High Pressure. *Sci. Rep.* **2016**, *6*, 26398.

(12) Michalopoulos, D. L.; Geusic, M. E.; Langridge-Smith, P. R. R.; Smalley, R. E. Visible Spectroscopy of Jet-Cooled Silicon Dicarbide: Geometry and Electronic Structure. *J. Chem. Phys.* **1984**, *80*, 3556−60.

(13) Koput, J. Ab Initio Potential Energy Surface and Vibration-Rotation Energy Levels of Germanium Dicarbide, GeC_2. *J. Comput. Chem.* **2018**, *39*, 1327−1334.

(14) Zingsheim, O.; Martin-Drumel, M.-A.; Thorwirth, S.; Schlemmer, S.; Gottlieb, C. A.; Gauss, J.; McCarthy, M. C. Germanium Dicarbide: Evidence for a T-Shaped Ground State Structure. *J. Phys. Chem. Lett.* **2017**, *8*, 3776−3781.

(15) Sunahori, F. X.; Wei, J.; Clouthier, D. J. Spectroscopic Identification of C_2P and C_2As, Two New Main Group Dicarbides. *J. Am. Chem. Soc.* **2007**, *129*, 9600−9601.

DOI: 10.1021/acs.jpclett.9b03297
J. Phys. Chem. Lett. 2020, 11, 88−92

(16) Fuentealba, P.; Savin, A. Electronic Structure and Bonding of the Ground State of Alkaline-Earth-Metal Monoxides and Carbides. *J. Phys. Chem. A* **2000**, *104*, 10882−10886.
(17) Boldyrev, A. I.; Simons, J. Structures of Small Magnesium Carbide Clusters: MgC_2, $(MgC_2)_2$, and $(MgC_2)_4$. *J. Phys. Chem. A* **1997**, *101*, 2215−2217.
(18) Koch, W.; Frenking, G.; Gauss, J.; Cremer, D.; Sawaryn, A.; Schleyer, P. v. R. Structures, Stabilities, and Bonding in CBe_2, C_2Be, and C_2Be_2. *J. Am. Chem. Soc.* **1986**, *108*, 5732−7.
(19) Ghouri, M. M.; Yareeda, L.; Mainardi, D. S. Geometry and Stability of Be_nC_m (n = 1−10; m = 1, 2, ..., to 11 - n) Clusters. *J. Phys. Chem. A* **2007**, *111*, 13133−13147.
(20) Chen, M. D.; Li, X. B.; Yang, J.; Zhang, Q. E.; Au, C. T. Parity Alternation in the Linear Ground-State Beryllium-Doped Carbon Clusters BeC_n^- (n = 1−8). *Int. J. Mass Spectrom.* **2006**, *253*, 30−37.
(21) Lee, T. J.; Kobayashi, R.; Handy, N. C.; Amos, R. D. Comparison of the Brueckner and Coupled-Cluster Approaches to Electron Correlation. *J. Chem. Phys.* **1992**, *96*, 8931−7.
(22) Patrick, A. D.; Williams, P.; Blaisten-Barojas, E. Energetics and Bonding in Beryllium Metalized Carbon Clusters. *J. Mol. Struct.: THEOCHEM* **2007**, *824*, 39−47.
(23) Ramondo, F.; Sanna, N.; Bencivenni, L. Ab Initio Geometries and Vibrational Frequencies of Coordination Structures of Inorganic Ion-Pairs. *J. Mol. Struct.: THEOCHEM* **1992**, *258*, 361−78.
(24) Mascaritolo, K. J.; Dermer, A. R.; Green, M. L.; Gardner, A. M.; Heaven, M. C. Photodetachment Spectroscopy of the Beryllium Oxide Anion, BeO^-. *J. Chem. Phys.* **2017**, *146*, 054301.
(25) Dermer, A. R.; Green, M. L.; Mascaritolo, K. J.; Heaven, M. C. Photoelectron Velocity Map Imaging Spectroscopy of the Beryllium Sulfide Anion, BeS^-. *J. Phys. Chem. A* **2017**, *121*, 5645−5650.
(26) Leon, I.; Yang, Z.; Liu, H.-T.; Wang, L.-S. The Design and Construction of a High-Resolution Velocity-Map Imaging Apparatus for Photoelectron Spectroscopy Studies of Size-Selected Clusters. *Rev. Sci. Instrum.* **2014**, *85*, 083106.
(27) Hock, C.; Kim, J. B.; Weichman, M. L.; Yacovitch, T. I.; Neumark, D. M. Slow Photoelectron Velocity-Map Imaging Spectroscopy of Cold Negative Ions. *J. Chem. Phys.* **2012**, *137*, 244201.
(28) Dick, B. Inverting Ion Images Without Abel Inversion: Maximum Entropy Reconstruction of Velocity Maps. *Phys. Chem. Chem. Phys.* **2014**, *16*, 570−580.
(29) Peterson, K. A.; Dunning, T. H., Jr Accurate Correlation Consistent Basis Sets for Molecular Core-Valence Correlation Effects: The Second Row Atoms Al-Ar, and the First Row Atoms B-Ne Revisited. *J. Chem. Phys.* **2002**, *117*, 10548−10560.
(30) Werner, H.-J.; Knowles, P. J.; Knizia, G.; Manby, F. R.; Schuetz, M. Molpro: a general-purpose quantum chemistry program package. *Wiley Interdisciplinary Reviews: Computational Molecular Science* **2012**, *2*, 242−253.
(31) Weinhold, F.; Landis, C. R.; Glendening, E. D. What is NBO Analysis and How is it Useful? *Int. Rev. Phys. Chem.* **2016**, *35*, 399−440.
(32) Schmider, H. L.; Becke, A. D. Chemical Content of the Kinetic Energy Density. *J. Mol. Struct.: THEOCHEM* **2000**, *527*, 51−61.
(33) Lu, T.; Chen, F. Multiwfn: A Multifunctional Wavefunction Analyzer. *J. Comput. Chem.* **2012**, *33*, 580−592.
(34) Frish, M. J.; et al. *Gaussian 09*, revision 1A; Gaussian Inc.: Wallingford, CT.
(35) Mayer, I.; Salvador, P. Overlap Populations, Bond Orders and Valences for 'Fuzzy' Atoms. *Chem. Phys. Lett.* **2004**, *383*, 368−375.

DOI: 10.1021/acs.jpclett.9b03297
J. Phys. Chem. Lett. 2020, 11, 88−92